Geosciences Journal
Vol. 15, No. 4, p. 349 − 357, December 2011
DOI 10.1007/s12303-011-0037-5

Diverse exhumation of the Mesozoic tectonic belt within the Yangtze Plate, China, determined by apatite fission-track thermochronology

Xiaoming Li*
Yehua Shan
Guangzhou Institute of Geochemistry, the Chinese Academy of Sciences, Guangzhou 510640, China

ABSTRACT: New and mostly published apatite fission-track (AFT) data are compiled to reveal the exhumation of the Mesozoic tectonic belt (MTB) within the Yangtze Plate, China. New AFT ages ranging from 51 ± 3 to 108 ± 5 Ma with mean measured track lengths between 11.8 ± 1.6 and 12.8 ± 2.0 μm, are obtained for the bedrock samples collected along a southeast to northwest transect across the MTB, including the exceptional Huangling Dome in the northern Yangtze Plate. The diverse, involving the first rapid, following by a slow, and the final accelerating, cooling and inferred exhumation from the Late Mesozoic to the Cenozoic have been identified in the study region based on the AFT data and modeling. The onset of exhumation is earlier in the Huangling Dome than in the southeastern and northwestern MTB, and in the southeastern MTB than in the northwestern MTB. Similarly, the final stage of accelerating exhumation seemed to start earlier in the Huangling Dome than in the southeastern and northwestern MTB, but in the northwestern MTB than in the southeastern MTB. The diverse exhumation of the MTB should have been attributed to the far-field effect of the Pacific plate subduction in the Cretaceous to the east, and to the eastward and southeastward tectonic escape from the Tibetan plateau imposed by the India-Eurasia collision since ~55 Ma to the west.

Key words: apatite fission-track, diverse exhumation, Mesozoic tectonic belt, geodynamics

1. INTRODUCTION

The Mesozoic tectonic belt (MTB) between the southeastern Wuling-Xuefeng Mountains and the eastern Sichuan Basin (Fig. 1) is an intraplate fold belt within the Yangtze Plate of South China. Magmatic and metamorphic activities have been absent since the Mesozoic. The belt has a structural style of chevron anticlines and thrusts in the west to chevron synclines and thrusts in the east, presumably due to the switch of thin-skinned to thick-skinned tectonics. Consequently, this led to the tendency of an increasing age of exposed rocks from the west to the east in the MTB.

There have been lots of studies and many controversies on the deformation style and the formation age of the MTB, and they are summarized below.

(1) After structural analysis of some anticlines, Yan et al. (2003, 2009) considered the multi-layer over-thrust system to develop in the Middle Jurassic to Late Cretaceous as part of an intracontinental orogen within the Yangtze Plate as a result of indentation tectonics following the Early Mesozoic collision of the North China and South China blocks.

(2) Wang et al. (2005) reckoned that the deformation of Xuefengshan tectonic belt and the eastern Sichuan foreland to the west occurred between the Middle Triassic and the Early Jurassic on the basis of $^{40}Ar/^{39}Ar$ dating and geological observations.

(3) Based upon a systematic collection of isotopic ages of magmatic intrusions, sedimentary facies, and structural deformation, Li and Li (2007) proposed that as a postorogenic magmatic province, the 1300-km-wide intracontinenta1 orogen in South China was formed during 250–150 Ma by a flat-slab subduction of the Pacific plate to the east.

(4) Hu et al. (2009) qualified the formation time of the tectonic belt was in a short interval between the Late Jurassic and Early Cretaceous by the stratigraphic unconformity.

Summarily, the MTB formed in the Mesozoic was basically consentaneous, but subsequent exhumation process remains poorly understood. The uplift and denudation of the MTB since the Late Mesozoic (at least the Late Cretaceous) have been generally recognized (Hu et al., 2006; Richardson et al., 2008, 2010; Shen et al., 2009; Mei, 2010; Tian et al., 2011). However, the age and rate of the exhumation, especially the variation in the different sections of the MTB are still poorly constrained.

Apatite fission-track (AFT) dating is an effective method to determine the history of the exhumation and the pattern of tectonic geomorphology in the upper crust. It has been successfully applied to study the spatial and temporal pattern of the exhumation since the Mesozoic in Alps, Appalachia, Andes, Qinghai-Tibetan Plateau, Qingling-Dabie-Sulu etc. (e.g., Gleadow and Fitzgerald, 1987; Johnson, 1997; Gallagher et al., 1998; Willet et al., 2003; Hu et al., 2006; Richardson et al., 2008, 2010; Wang et al., 2009). Thus, in this study, we compile new and mostly published AFT data to better constrain the age and rate of the cooling of the Mesozoic tectonic belt (MTB) within the Yangtze Plate, provide firmer constraints on the exhumation history. The data are also used to discuss the possible exhumation geodynamics.

*Corresponding author: lixm@gig.ac.cn

2. GEOLOGICAL SETTING

The MTB is situated in the northwestern part of the Yangtze Plate. To the north, the Yangtze plate is separated from the North China Craton by the Late Paleozoic to the Early Mesozoic Qingling-Dabie orogenic belt (QDOB), and to the west from the eastern margin of the Tibetan Plateau by the Longmenshan-Yanyuan thrust belt (LYTB) (Fig. 1).

The Wuling-Xuefeng Mountains in the southeastern part of the MTB is an east-northeast to northeast-trending intraplate deformation belt. It comprises a series of arcuate anticlines and synclines, exhibiting the chevron syncline-thrust system. The Banxi Group and its equivalents of Meso- to Neo-proterozoic age in the Yangtze Plate comprise the metamorphic basement (Yan et al., 2003). The sedimentary cover consists mainly of folded Paleozoic and Lower Mesozoic strata of shallow-marine origin. Jurassic, Cretaceous and Cenozoic strata are composed entirely of terrigenous clastic sequences (HNBGMR, 1988).

On the west, the Huayun thrust separates the Sichuan Basin and the MTB. Towards the southeast, thin-skinned deformation is gradually replaced at the Cili-Baoqin detach-

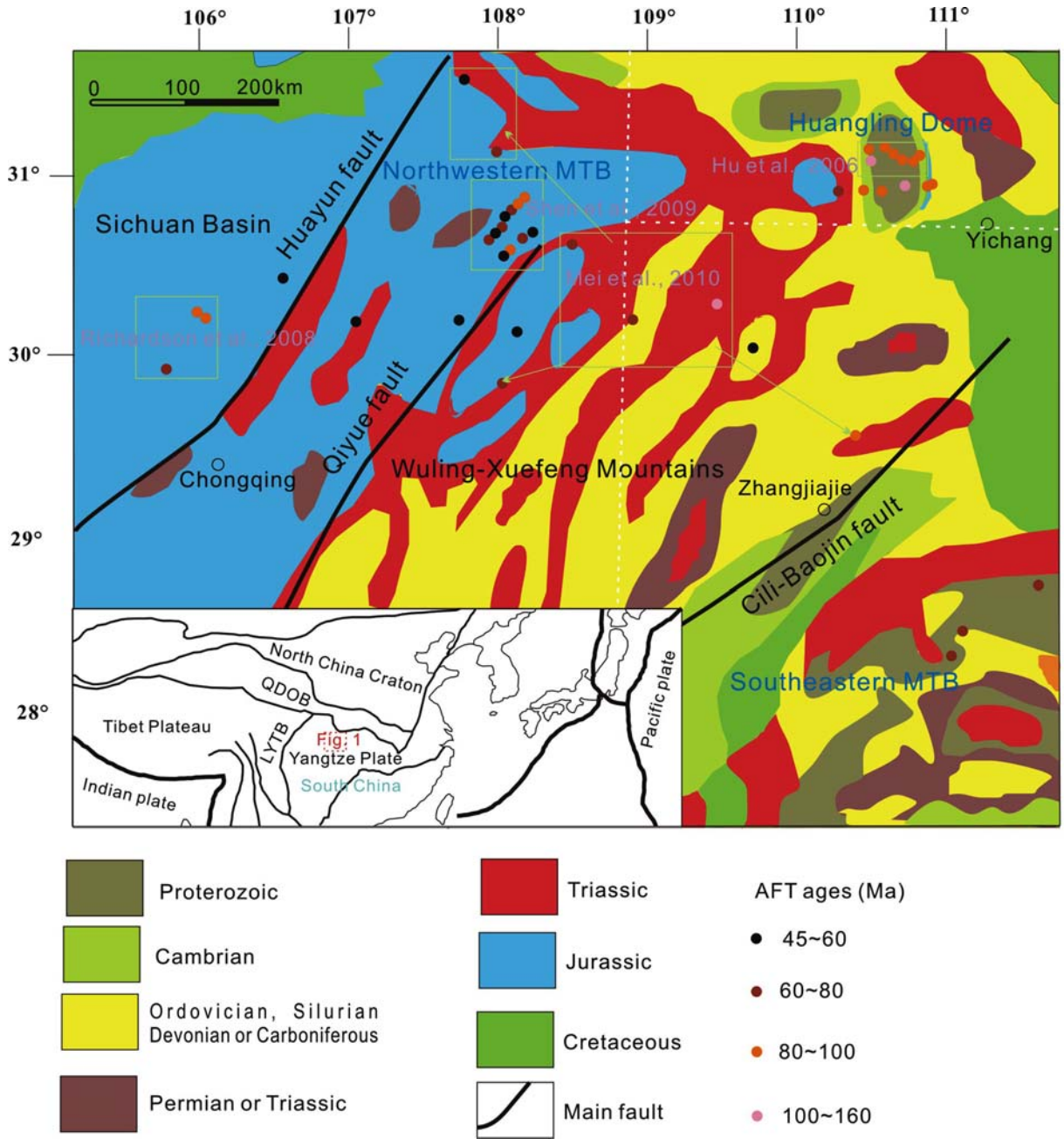

Fig. 1. Sketch of the MTB, China (Modified after Ma et al., 2002), and a compilation of AFT ages from Hu et al. (2006), Richardson et al. (2008), Shen et al. (2009, Mei et al. (2010), and this study (the unspecified provenance).

ment fault by thick-skinned deformation characterized by the Xuefeng and Wuling nappes and numerous klippen. The thin-skinned belt is structurally overlain by the thick-skinned belt on which Jurassic red beds rest unconformably (Yan et al., 2003).

As is different from a series of anticlines and synclines in the southeastern and northwestern MTB, the Huangling Dome in the northern Yangtze Plate, near the QDOB, has an exhumed core of the basement, or the Neoarcheozoic and Paleoproterozoic high-grade metamorphic Kongling group, away from which the Paleozoic and Mesozoic rocks crop out (Fig. 1) (HBBGMR, 1990).

3. SAMPLING AND EXPERIMENTAL METHODS

In this study, fourteen representative samples of fresh samples from a southeast to northwest transect across the MTB, including the transmeridional Huangling Dome were collected for AFT analysis (Fig. 1, Table 1) to address their cooling, and inferred exhumation history. Most samples are of Jurassic in stratigraphic age, and some of Archeozoic, Proterozoic, Siniria, Permian or Cretaceous (Table 1). These samples are fine- to coarse-grain sandstone, granitic gneiss or granite, without any significant neotectonic and magmatic overprinting. Efforts have been paid to avoid possible thermal effect related to active faults.

A portable GPS was used to measure the longitude and latitude of each sampling location with precision in the order of 10 m, and the elevation with precision in the order of 5m. This sampling strategy allows comparing the distribution of the AFT ages with the relative locations and elevations of the samples in order to estimate the variations in the cooling, and the inferred exhumation history.

Apatite crystals were obtained by crushing, sieving, magnetic and heavy liquids separation techniques. Apatite crystals were mounted by epoxy resin. These prepared samples were carefully ground and polished to an optical finish to expose internal grain surfaces. Apatite spontaneous fission tracks were revealed by 5.5 M HNO_3 at 21 °C for 20 seconds (Carlson et al., 1999).

AFT ages were analyzed by using external detector method (Hurford and Green, 1983). The mounts were covered with a flake of low-U muscovite, packed for irradiation, together with standard uranium dosimeter glass SRM612 and standard known age sample FCT (27.8 ± 0.7Ma) (Hurford and Green, 1983), and irradiated in a well-thermalized (Cd for Au > 100) neutron flux 492 Swim reactor, Chinese Institute of Atomic Energy. After irradiation, muscovites were etched in 40% HF at 25 °C for 20 minutes to reveal induced fission tracks. Maximum etch pit dimensions (*Dpar*) were concurrently monitored as a representative of their chlorine content. Only those crystals with prismatic sections parallel to the c-crystallographic axis were accepted for *Dpar* analysis, because of their high etching efficiency. The AFT ages were calculated following the method recommended by Hurford (1990), using the zeta calibration method (Hurford and Green, 1983). The AFT ages were calculated using the Trackkey software® (Dunkl, 2002). Ages quoted are central fission track ages with one standard error. Zeiss Axioplan microscope at ×1250 magnification with AUTOSCAN system was used to observe and measure the spontaneous and induced densities of AFT populations, as well as confined lengths and the related *Dpar* values of apatite fission tracks.

4. RESULTS

4.1. FT Data

The measured data, including the central ages of AFT (as AFT ages in this study), the mean measured track lengths (MTL) and the *Dpar* values of AFT are listed in Table 1, whilst the representative plots of *Lc* (c-axis projected track length) with unimodal distribution are illustrated in Figure 2. The measured AFT ages range from 51 ± 3 to 57 ± 3 Ma in the northwestern EMTB, 62 ± 5 to 70 ± 7 Ma in the southeastern EMTB, and 87 ± 9 to 108 ± 5 Ma in the Huangling Dome. The mean measured track lengths range from 11.8 ± 1.6 to12.8 ± 2.0 μm, and a mean *Dpar* value of 1.5 ± 0.1 to 1.8 ± 0.2 μm (Table 1).

To better interpret the significance of our data, we modeled four representative AFT data sets with sufficient track lengths to quantify the timing and amount of cooling at specific locations. Their time-temperature paths are most likely to reveal the exhumation history of the MTB, as the chosen samples are basically evenly distributed in the study region (Table 1).

Time-temperature histories were calculated by the inverse modeling approach using the version 1.6.7 (2009) of HeFTy (Ketcham, 2005) with a multi-compositional annealing model (Ketcham et al., 2007b) and the *Dpar* value as kinetic parameter. Models were run using c-axis projected lengths (Ketcham et al., 2007a), and initial track lengths were calculated according to the mean *Dpar* value of each sample using the formula of Carlson et al. (1999). The thermal history modeling results, as well as the plots of *Lc* distribution, are illustrated in Figure 2, from which it infers that both the measured and the model AFT ages and lengths are consistent within the scope of standard errors. Based on GOF (Goodness of fit) > 0.5 by the Kolmogorov-Smimov test, the c-axis projected and the model track lengths vary from 12.4 to 13.1 μm, and 12.6 to 13.2 μm, respectively; both the measured and the model AFT ages range from 57 to 108 Ma. Clearly, the four time-temperature cooling curves exhibit diverse patterns.

4.2. Cooling History Analysis of Each Sample

The probability of χ^2 values for (n–1) (n is number of

Table 1. Apatite fission track data from the Mesozoic tectonic belt within the Yangtze Plate

Sample No	Latitude E	Longitude N	Elevation /m	Rock type	Formation era*	*n*	$\rho_s/\times10^5cm^{-2}$ (N_s)	$\rho_i/\times10^5cm^{-2}$ (N_d)	$\rho_d/\times10^5cm^{-2}$ (N_d)	Central age (Ma)±1σ	P(χ^2) /%	MTL±1σ /μm	No. of tracks	Mean Dpar ±1s/μm
Northwestern MTB														
JX-163	106°51.079′	30°28.262′	314	Sandstone	J	15	12.57(432)	23.51(808)	5.59(5245)	51 ± 3	48			
JX-166	107°20.480′	30°12.767′	388	Sandstone	J	20	11.40(613)	18.53(996)	5.30(4967)	56 ± 3	98	12.5 ± 1.6	56	1.6 ± 0.2
JX-168	108°02.007′	30°18.739′	251	Siltstone	J	20	20.18(1211)	33.68(2021)	5.59(5245)	57 ± 3	74	12.3 ± 1.9	101	1.8 ± 0.2
JX-170	108°26.008′	30°15.338′	1303	Sandstone	J	14	11.91(469)	20.22(796)	5.59(5245)	56 ± 4	87			
Southeastern MTB														
JX-172	109°42.970′	30°35.053′	569	Siltstone	S	23	16.18(526)	27.29(887)	5.59(5245)	56 ± 4	99	12.2 ± 1.8	81	1.7 ± 0.2
JX-188	111°16.248′	28°44.260′	45	Metasandstone	Pt	7	25.60(208)	34.59(281)	5.59(5245)	70 ± 7	89			
JX-193	111°03.222′	28°29.258′	306	Metasandstone	Z	22	10.23(646)	15.73(993)	5.59(5245)	62 ± 4	94	11.8 ± 1.6	51	1.7 ± 0.2
JX-195	111°01.670′	28°26.605′	464	Metasiltstone	Pt	7	17.13(364)	22.99(509)	5.30(4967)	62 ± 5	83			
Huangling Dome														
JX-174	110°12.824′	31°12.824′	269	Siltstone	J	24	11.54(808)	16.21(1135)	5.30(4967)	64 ± 3	98	11.9 ± 1.7	53	1.5 ± 0.1
JX-176	110°56.130′	31°11.647′	472	Granite	γ_2	20	13.72(832)	13.67(829)	5.30(4967)	90 ± 5	100	12.4 ± 1.7	53	1.6 ± 0.2
JX-178	111°02.004′	31°10.367′	747	Granitic gneiss	γ_2	20	17.28(1501)	17.05(1481)	5.30(4967)	91 ± 4	25	12.1 ± 1.8	105	1.6 ± 0.1
JX-183	111°13.632′	31°05.798′	405	Granite	γ_2	20	20.31(1333)	16.87(1107)	5.30(4967)	108 ± 5	99	12.5 ± 1.9	105	1.7 ± 0.2
JX-184	111°33.330′	31°10.853′	168	Siltstone	K_2	8	17.13(364)	17.69(376)	5.30(4967)	87 ± 7	90			
JX-186	111°44.172′	31°10.032′	389	Siltstone	J	21	13.65(870)	12.99(828)	5.30(4967)	95 ± 5	98	12.8 ± 2.0	52	1.5 ± 0.1

n: number of crystals counted; ρ_s: spontaneous track density of a sample; N_s: number of tracks counted to determine ρ_s; ρ_i: induced track density of a sample measured in a muscovite external detector; N_i: number of tracks counted to determine ρ_i; ρ_d: induced track density of glass dosimeter SRM612 measured in a muscovite external detector; N_d: number of tracks counted to determine ρ_d; MTL±1σ: mean measured fission track lengths with one standard deviation; P(χ^2): probability of equaling or exceeding χ^2(n-1) degrees of freedom; *: after HNBGMR, 1988; HBBGMR, 1990; SCBGMR , 1991. Ages determined by external detector method using zeta values of 342.1 ± 7.8.

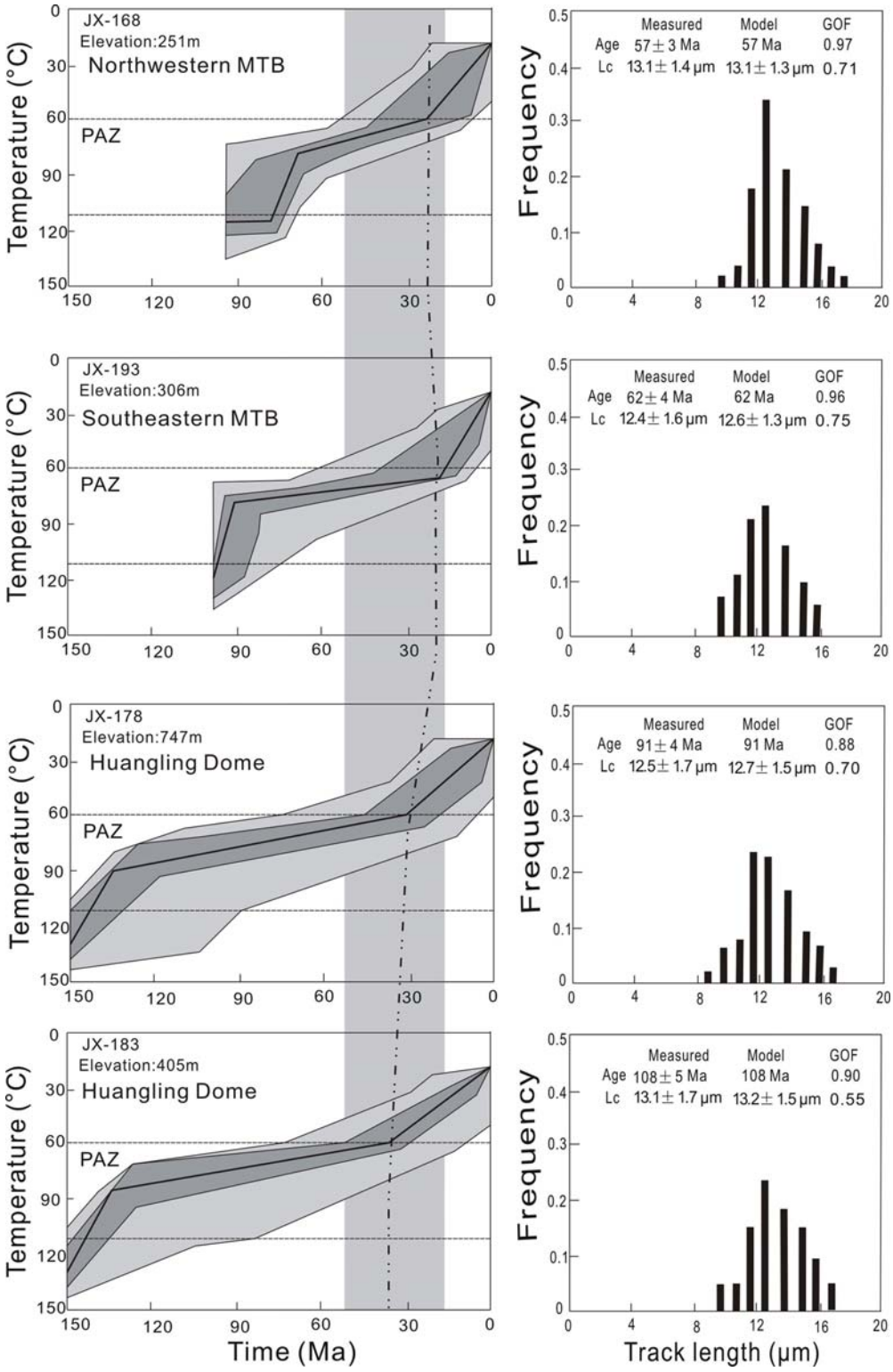

Fig. 2. Representative plots of time-temperature paths modeled by the AFT data and the c-axis projected track (*Lc*) distributions. Thermal modeling of AFT length and age data modeled time-temperature paths for four apatite samples, computed with the version 1.6.7 (2009) of HeFTy program by Ketcham (2005). Temperature ranges between 110 and 60 °C delineate apatite partial annealing zone, defined as temperature interval in which majority of track length shortening take place. Parameters and variables include: (1) the constant present surface temperature of 20 °C, (2) the kinetic variable of *Dpar* to be input, (3) measured track lengths and the related angles to be input, and (4) c-axis projected lengths (Ketcham et al., 2007a) and default initial track lengths according to $L_{0,c,mod} = 16.10 + 0.205\ Dpar$ (μm) (Carlson et al., 1999; Ketcham et al., 2007a, 2007b). We modeled 10,000 paths for each plot. Thick lines show the best-fit solutions obtained for these model runs, and dark-grey and light-grey colors show the good-fit solutions and the accept-fit solutions, respectively.

crystals counted) degrees of freedom in AFT scatter, or $P(\chi^2)$, is far greater than 5% (Table 1), indicating that the ages of apatite crystals can be classified as a single population for each sample.

Except for sample JX-184, all the samples have an AFT age of <120 Ma, markedly younger than their formation ages of their host-rocks (>120 Ma) (HNBGMR, 1988; HBBGMR, 1990; SCBGMR, 1991). Therefore, they represent the cooling ages of the samples during the uplift and denudation processes owing to their negligibly affected by magmatic or tectonic activities since the late Mesozoic (HNBGMR, 1988; HBBGMR, 1990; SCBGMR, 1991).

Because the exceptional sample JX-184 has an AFT age (87 ± 7 Ma) no less than the stratigraphic age of upper Cretaceous, the AFT age maybe reveals the information of source area, not the cooling, and inferred exhumation history; thus we hereinafter do not take the sample JX-184 into account. The other apatite samples must have experienced significant track annealing and a relatively long-term lingering in the AFT partial annealing zone owing to the evident shortening of apatite fission tracks (Table 1).

Figure 2 indicates that the time-temperature cooling curves exhibit multi-stages or episodic patterns, including two rapid and one slow cooling in the MTB since the Late Mesozoic.

4.3. Comparison of Cooling History among Various Locations

Table 1 lists a spread of new AFT ages at the sampling locations, suggesting a diverse exhumation in the MTB since the Late Mesozoic. Moreover, Table 1 manifests the weak relationship between the AFT ages and the sample elevations, not as would be expected from a region experiencing simple exhumation.

Figure 3 exhibits the histograms of the apatite fission track age distribution in the northwestern MTB, in the southeastern MTB and in the Huangling Dome, in comparison with the AFT ages of surface rocks in the study region by Hu et al. (2006), Richardson et al. (2008), Shen et al. (2009), Mei et al. (2010), and this study. Evidently, the AFT ages are divisible into three clusters of ~65 Ma in the northwestern MTB, ~75 Ma in the southeastern MTB and ~95 Ma in the Huangling Dome (Fig. 3).

These AFT ages suggest that these samples once cooled to the closure temperatures (~100 °C) of AFT, and exhumed to the equivalent burying depths in the northwestern MTB in ~65 Ma, in the southeastern MTB in ~75 Ma, and in the Huangling Dome in ~95 Ma, respectively.

Figure 2 illustrates the cooling history of the MTB since the late Mesozoic. Based on the best-fit paths modeled by the AFT data, it has probably experienced an episodic cooling since the Late Mesozoic as follows:

(1) The first rapid cooling probably occurred in the northwestern MTB ~80 Ma ago, in the southeastern MTB ~100 Ma ago, and in the Huangling Dome ~150 Ma ago.

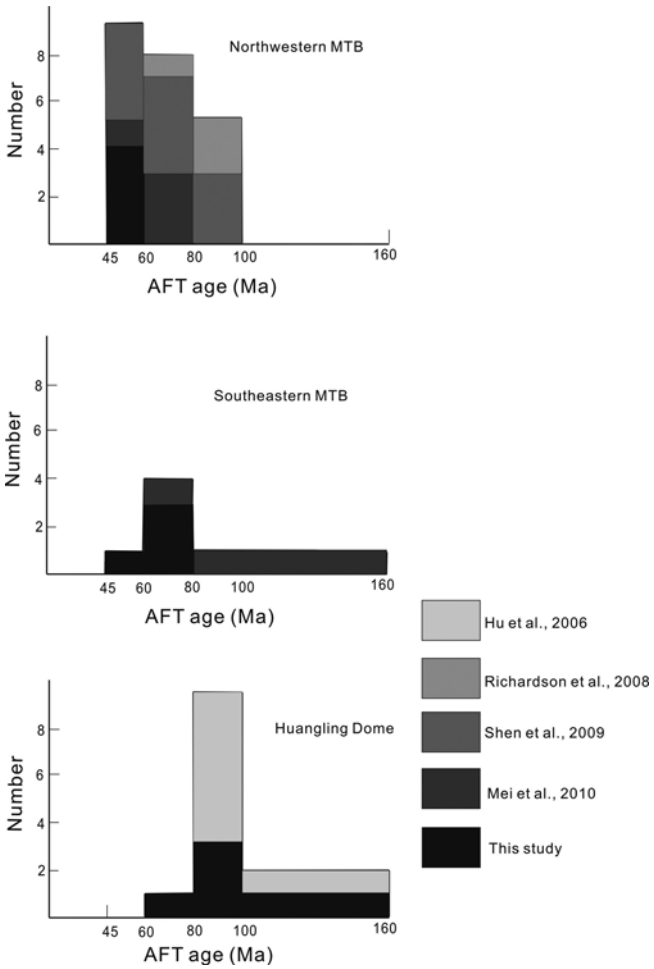

Fig. 3. Histograms of apatite fission track ages from Hu et al. (2006), Richardson et al. (2008), Shen et al. (2009), Mei et al. (2010), and this study.

(2) Subsequent slow cooling maybe took place in the northwestern MTB during ~80–25 Ma, in the southeastern MTB during ~100–15 Ma, and in the Huangling Dome during ~150–35 Ma.

(3) A second rapid cooling possibly arose in the northwestern MTB after ~25Ma, in the southeastern MTB after ~15 Ma, and in the Huangling Dome after ~35 Ma.

5. DISCUSSION

The AFT analyses performed within the MTB allowed us to reconstruct their exhumation history and deduce their geodynamics implications over the period the Late Mesozoic to Recent time.

5.1. Diverse Exhumation

From the histograms of apatite fission track ages (Fig. 3)

and best-fit paths modeled by the AFT data (Fig. 2), several conclusions can be drawn and summarized below.

(1) The ~65 Ma of AFT ages and the modeling result of JX-168 from the northwestern MTB means that the samples were exhumed through the partial annealing zone of AFT as a simple block, and the main upper part of the northwestern MTB remained at temperatures lower than ~110 and ~60 °C after cooling episode in ~80 Ma and in ~25 Ma, respectively (Fig. 2). Assuming a steady-state paleogeothermal gradient of 30 °C/km, the present surface of the tectonic belt should have been buried at a depth of ~2–3 and ~1–2 kilometres in the periods of the Late Cretaceous and the Oligocene, respectively.

(2) The ~75 Ma of AFT ages and the modeling result of JX-193 from the southeastern EMTB means that the samples were exhumed through the partial annealing zone of AFT as a simple block, and the main upper part of southeastern MTB remained at temperatures lower than ~110 and ~60 °C after cooling episode in ~100 Ma and in ~15 Ma, respectively (Fig. 2). Assuming a steady-state paleogeothermal gradient of 30 °C/km, the present surface of southeastern MTB should have been buried at a depth of ~2–3 and ~1–2 kilometres in the periods of the Late Cretaceous and the Miocene, respectively.

(3) The ~95 Ma of AFT ages and the modeling results of JX-178 and JX-183 (their AFT ages are overlapped at $\pm 2\sigma$ level) from the Huangling Dome means that the samples were exhumed through the partial annealing zone of AFT as a simple block, and the main upper part of the Huangling Dome remained at temperatures lower than ~110 and ~60 °C after cooling episode in ~140 Ma and in ~35 Ma, respectively (Fig. 2). Assuming a steady-state paleogeothermal gradient of 30 °C/km, the present surface of the Huangling Dome should have been buried at a depth of ~2–3 and ~1–2 kilometres in the periods of the Early Cretaceous and the Eocene, respectively.

Apparently, the diverse cooling, and inferred exhumation occurred in the MTB from the aforementioned conclusions. The onset of exhumation is earlier in the Huangling Dome than in the southeastern MTB and in the northwestern MTB, and in the southeastern MTB than in the northwestern MTB. The final cooling and inferred exhumation in the Huangling Dome since ~35 Ma possibly started earlier than in the southeastern MTB since ~15 Ma and in the northwestern MTB since ~25 Ma, but in the northeastern MTB since ~25 Ma than in the southeastern MTB since ~15 Ma. This is basically concordant to the final accelerated exhumation in the Huangling Dome and the onset of incision in the Three Gorges after 40 Ma (Hu et al., 2006; Richardson et al., 2010). This is also not contrary to the final cooling and inferred exhumation after ~30 Ma in the northeastern Sichuan Basin constraint from low-temperature thermochronology profiles (Tian et al., 2011), but possibly reveals the final cooling and inferred exhumation propagation from the edge of the northeastern Sichuan Basin to the MTB.

In case according to the good-fit path envelopes modeled by the AFT data, the final cooling, and inferred exhumation after ~15–50 Ma in the Huangling Dome is approximately identical with those after ~15–50 Ma in the northwestern and southeastern MTB (Fig. 2). This mainly contains the final cooling and inferred exhumation since ~30 Ma in the northeastern Sichuan Basin constraint from low-temperature thermochronology profiles (Tian et al., 2011). Accordingly, the final cooling and inferred exhumation seemed to vary slightly in the northeastern Sichuan Basin and in the MTB.

Further, this diverse exhumation of the MTB is consistent with the following aspects: (1) the onsets of uplifting for different tectonic units in the Mid-upper Yangtze area decrease westward (Yuan et al., 2010); (2) the Huangling Dome was formed in 165–100 Ma, in combination with the features of detrital AFT ages, thermal history and strata distribution etc. (Liu et al., 2009); and (3) the Mesozoic intracontinental deformation in western Hunan and Hubei Provinces to eastern Sichuan Province was progressive with a large width and a long diachronous interval (Mei et al., 2010).

In short, the onset of exhumation is earlier in the Huangling Dome than in the southeastern and northwestern MTB, and in the southeastern MTB than in the northwestern MTB. The final accelerating cooling and exhumation possibly started earlier in the Huangling Dome than in the southern and northwestern MTB, but in the northwestern MTB than in the southeastern MTB.

5.2. Possible Exhumation Geodynamics

Our results reveal the diverse cooling and inferred exhumation in the MTB since the Late Mesozoic, and the various exhumed mechanisms may be deduced in the following.

The northwestward subduction of the Pacific plate during 80–100 Ma (e.g., Sun et al., 2007) led to the onset of exhumation from the southeastern to northwestern MTB in the Late Cretaceous. However, that the exceptional Huangling Dome experienced rapid uplift and denudation in the Early Cretaceous might have resulted from a combination of the Mesozoic lateral extrusion and rotation of the QDOB and clockwise rotation of the Yangtze Plate (e.g., Meng and Zhang, 2000; Tan et al., 2007), and an abrupt change from southwest to northwest in the drifting direction of the subducting Pacific plate at ~125 Ma (e.g., Sun et al., 2007).

The final rapid exhumations in the northwestern MTB after ~25 Ma, in the southeastern MTB after ~15 Ma, and in the Huangling Dome after ~35 Ma were dominantly caused by the eastward and southeastward tectonic escape from the Tibetan Plateau imposed by the India-Eurasian collision and corresponding uplift of the Tibetan Plateau commenced ~55 Ma (e.g., Klootwijk et al., 1992; Rowley,

1996).

This possible exhumed mechanism can better interpret the AFT ages and modeling of the MTB, including the exceptional Huangling Dome.

6. CONCLUSIONS

The AFT ages and thermal history modeling results reveal that the MTB has experienced a three-stage cooling, and inferred exhumation history spanning the Late Mesozoic and Cenozoic eras. An obviously diverse exhumation of the MTB has been recognized from the AFT ages and modeling time-temperature paths since the Late Mesozoic as follows:

(1) The first rapid cooling and inferred exhumation took place earlier in the Huangling Dome than in the southeastern MTB and in the northwestern MTB, and in the southeastern MTB than in the northwestern MTB.

(2) The final accelerated cooling and inferred exhumation possibly occurred earlier in the Huangling Dome than in the southeastern MTB and in the northwestern MTB, but in the northwestern MTB than in the southeastern MTB.

(3) The slow cooling and inferred exhumation arose in the MTB in the interval of the two rapid cooling.

The diverse exhumation of the MTB should have been attributed to the far-field effect of the Pacific plate subduction in the Cretaceous to the east, and to the eastward and southeastward tectonic escape from the Tibetan plateau imposed by the India-Eurasia collision after ~55 Ma to the west.

ACKNOWLEDGMENTS: This work was financially supported by the National Key Project No. 2008ZX05008 and the National Natural Science Foundation of China No. 41072158. We thank two anonymous reviewers and Editor Dr. Kyoungwon Kyle Min for their constructive comments and suggestions that improve the manuscript significantly. This is contribution No. IS-1411 from GIGCAS.

REFERENCES

Carlson, W.D., Donelick, R.A., and Ketcham, R.A., 1999, Variability of apatite fission-track annealing kinetics: Experimental results. American Mineralogist, 84, 1213–1223.

Dunkl, I, 2002, TRACKKEY: a Windows program for calculation and graphical presentation of fission track data. Computers & Geosciences, 28, 3–12.

Gallagher, K., Brown, R., and Johnson, C., 1998, Fission track analysis and its application to geological problems. Annual Review of Earth and Planetary Sciences, 26, 519–572.

Gleadow, A.J.W. and Fitzgerald, P.G., 1987, Uplift history and structure of the Transantarctic Mountains: New evidence from fission track dating of basement apatites in the Dry Valleys area, southern Victoria Land. Earth and Planetary Science Letters, 82, 1–14.

HBBGMR (Hubei Bureau of Geology and Mineral Resources), 1990, Regional Geology of Hubei Province. Geological Publishing House, Beijing, 645 p (in Chinese with English abstract).

HNBGMR (Hunan Bureau of Geology and Mineral Resources), 1988, Regional Geology of Hunan Province. Geological Publishing House, Beijing, 528 p (in Chinese with English abstract).

Hu, S.B., Raza, A., Min, K., Kohn, B.P., Reneirs, P.W., Ketcham, R.A., Wang, J.Y., and Gleadow, A.J.W., 2006, Late Mesozoic and Cenozoic thermotectonic evolution along a transect from the north China craton through the Qinling orogen into the Yangtze craton, central China. Tectonics, 25, TC6009, doi:10.1029/2006TC001985.

Hu, Z.Q., Zhu, G., Liu, G.S., and Zhang, B.L., 2009, The folding time of the eastern Sichuan Jura–type fold belt: Evidence from unconformity. Geological Review, 55, 32–42 (in Chinese with English abstract).

Hurford, A.J. and Green, P.F., 1983, The Zeta age calibration of fission-track dating. Isotope Geoscience, 1, 285–317.

Hurford, A.J., 1990, Standarization of fission track dating calibration: Recommendation by the Fission Track Working Group of the I.U.G.S. Subcommission on Geochronology. Chemical Geology, 180, 171–178.

Johnson, C., 1997, Resolving denudational histories in orogenic belts with apatite fission track thermochronology and structural data: An example from southern Spain. Geology, 25, 623–625.

Ketcham, R.A., 2005, Forward and inverse modeling of low-temperature thermochronometry data. Reviews in Mineralogy & Geochemistry, 58, 275–314.

Ketcham, R.A., Carter, A., Donelick, R.A., Barbarand, J., and Hurford, A.J., 2007a, Improved measurement of fission-track annealing in apatite using c-axis projection. American Mineralogist, 92, 789–798.

Ketcham, R.A., Carter, A., Donelick, R.A., Barbarand, J., and Hurford, A.J., 2007b, Improved modeling of fission-track annealing in apatite. American Mineralogist, 92, 799–810.

Klootwijik, C.T., Gee, J.S., Peirce, J.W., Smith, G.M., and McFadden, P.L., 1992, An early India-Asia contact; paleomagnetic constraints from Ninetyeast Ridge, ODP Leg 121. Geology, 20, 395–398.

Li, Z.X. and Li, X.H., 2007, Formation of the 1300-km-wide intracontinental orogen and postorogenic magmatic province in Mesozoic South China: A flat-slab subduction model. Geology, 35, 179–182.

Liu, H.J., Xu, C.H., Zhou, Z.Y., and Donelick,R.A., 2009, Constraint formation age (165–100 Ma) of Huangling dome from detrital apatite fission track thermochronology. Progress in Natural Sciences, 19, 1326-1332 (in Chinese).

Ma, L., Qiao, X., Min, L., Fan, B., Ding, X., and Liu, N., 2002, Geological atlas of China. Geological Publishing House, Beijing, 348 p.

Mei, L.F., Liu, Z.Q., Tang, J.G., Shen, C.B., and Fan, Y.F., 2010, Mesozoic intra-continental progressive deformation in western Hunan-Hubei-eastern Sichuan provinces of China: Evidence from apatite fission track and balanced cross-section. Earth Science-Journal of China University of Geosciences, 35, 161–174 (in Chinese with English abstract).

Meng, Q.R., and Zhang, G.W., 2000, Geologic framework and tectonic evolution of the Qinling orogen, central China. Tectonophysics, 323, 183–196.

Richardson, N.J., Densmore, A.L., Seward, D., Fowler, A., Wipf, M., Ellis, M.A., Yong, L., and Zhang, Y., 2008, Extraordinary denudation in the Sichuan Basin: Insights from low temperature thermochronology adjacent to the eastern margin of the Tibetan Plateau. Journal of Geophysical Research, 113, B04409, doi:10.1029/2006JB004739.

Richardson, N.J., Densmore, A.L., Seward, D., Wipf, M., and Yong, L., 2010, Did incision of the Three Gorges begin in the Eocene? Geology, 38, 551–554.

Rowley, D., 1996, Age of initiation of collision between India and Asia: a review of stratigraphic data. Earth and Planetary Science Letters, 145, 1–13.

SCBGMR (Sichuan Bureau of Geology and Mineral Resources), 1991, Regional Geology of Sichuan Province. Geological Publishing House, Beijing, 680 p. (in Chinese with English abstract).

Shen, C.B., Mei, L.F., and Xu, S.H., 2009, Fission track dating of Mesozoic sandstones and its tectonic significance in the Eastern Sichuan Basin, China. Radiation Measurements, 44, 945–949.

Sun, W.D., Ding, X., Hu, Y.H., and Li, X.H., 2007, The golden transformation of the Cretaceous plate subduction in the west Pacific. Earth and Planetary Science Letters, 262, 533–542.

Tan, X., Kodama, K.P., Gilder, S., Courtillot, V., and Cogne, J.-P., 2007, Palaeomagnetic evidence and tectonic origin of clockwise rotations in the Yangtze Fold Belt, south China block. Geophysical Journal International, 168, 48–58.

Tian, Y.T., Zhu, C.Q., Xu, M., Rao, S., Kohn, B.P., and Hu, S.B., 2011, Post-Early Cretaceous denudation history of the northeastern Sichuan Basin: constraints from low-temperature thermochronology profiles. Chinese Journal of Geophysics, 54(3), 807–816 (in Chinese with English abstract).

Wang, Q., Li, S., and Du, Z., 2009, Differential uplift of the Chinese Tianshan since the Cretaceous: constraints from sedimentary petrography and apatite fission-track dating. International Journal of Earth Sciences, 98, 1341–1363.

Wang, Y.J., Zhang, Y.H., Fan, W.M., and Peng, T.P., 2005, Structural signatures and 40Ar/39Ar geochronology of the Indosinian Xuefengshan transpressive belt, South China interior. Journal of Structural Geology, 27, 985–998.

Willett, S.D., Fisher, D., Fuller C., Yeh, E.C., and Lu, C.Y., 2003, Erosion rates and orogenic-wedge kinematics in Taiwan inferred from fission-track thermochronometry. Geology, 31, 945–948.

Yan, D.P., Zhou, M.F., Song, H.L., Wang, X.W., and Malpas, J., 2003, Origin and tectonic significance of a Mesozoic multi-layer over-thrust system within the Yangtze Block (South China). Tectonophysics, 361, 239–254.

Yan, D.P., Zhang, B., Zhou, M.F., Wei, G.Q., Song, H.L., and Liu, S.F., 2009, Constraints on the depth, geometry and kinematics of blind detachment faults provided by fault propagation folds: an example from the Mesozoic fold belt of South China. Journal of Structural Geology, 31, 150–162.

Yuan, Y.S., Sun, D.S., Zhou, Y., Wang, X.W., Li, S.J., Zhang, R.Q., and Wo, Y.J., 2010, Determination of onset of uplifting for the Mid-upper Yangtze area after Indosinian event. Chinese Journal of Geophysics, 53, 362–369 (in Chinese with English abstract).

Manuscript received May 12, 2011
Manuscript accepted October 28, 2011